


Article

Reliability Analysis on Multiple Failure Modes of Underground Chambers Based on the Narrow Boundary Method

Huadong Yin ^{1,*} , Daobing Zhang ^{1,*}, Jiahua Zhang ², Biao Yu ¹ and Xiaomeng Yuan ¹

¹ School of Resource Environment and Safety Engineering, Hunan University of Science and Technology, Xiangtan 411201, China

² Work Safety Key Lab on Prevention and Control of Gas and Roof Disasters for Southern Coal Mines, Hunan Provincial Key Laboratory of Safe Mining Techniques of Coal Mines, Hunan University of Science and Technology, Xiangtan 411201, China

* Correspondence: 21300102001@mail.hnust.edu.cn (H.Y.); dbzhang@hnust.edu.cn (D.Z.)

Abstract: This paper proposes to study the stability of underground chambers while taking into account the nonlinear characteristics of geotechnical materials and pore water. According to the upper bound theorem of nonlinear limit analysis and the reliability theory, the failure mode and reliability model of underground chambers are established considering the pore water effect. The upper bound solution expression of the surrounding rock pressure in the underground chamber is deduced. The variation law of the surrounding rock pressure is analyzed under different parameters. At the same time, based on the narrow boundary method considering the correlation of multiple failure modes, the influence of different random parameters on the failure probability and reliability index of underground chambers is studied. The results show that the water-level line height, pore water pressure coefficient and Hoek-Brown failure criterion parameter have significant effects on the surrounding rock pressure and underground chamber reliability. In addition, the concept of the safety level is introduced, and the minimum-support force range of the underground chamber with safety level 1 is obtained under different random parameters. The research results can provide a theoretical basis and reference for the structural safety evaluation of underground chambers.

Keywords: underground chamber; surrounding rock pressure; reliability; narrow boundary method; pore water



Citation: Yin, H.; Zhang, D.; Zhang, J.; Yu, B.; Yuan, X. Reliability Analysis on Multiple Failure Modes of Underground Chambers Based on the Narrow Boundary Method. *Sustainability* **2022**, *14*, 12045. <https://doi.org/10.3390/su141912045>

Academic Editors: Chengyu Xie, Yaguang Qin and Qingfa Chen

Received: 22 July 2022

Accepted: 8 September 2022

Published: 23 September 2022

Publisher's Note: MDPI stays neutral with regard to jurisdictional claims in published maps and institutional affiliations.



Copyright: © 2022 by the authors. Licensee MDPI, Basel, Switzerland. This article is an open access article distributed under the terms and conditions of the Creative Commons Attribution (CC BY) license (<https://creativecommons.org/licenses/by/4.0/>).

1. Introduction

With the large-scale utilization of ground space around the world, the original ground space has long been unable to meet development needs. The use of subterranean space and its development have reached the status of national development strategies [1,2], resulting in a large number of underground chamber projects. After the underground chamber is excavated, the original stress balance condition of the rock mass is broken, and the surrounding rock will redistribute the stress, causing various deformations and damages such as tension, compression and shearing of the surrounding rock [3,4]. Therefore, it is very important to maintain the stability of the underground chamber as the surrounding rock pressure of the chamber is studied under the limit state.

In order to ensure that performing the normal function of the underground chamber during the service cycle, it is necessary to clarify the ultimate load of the surrounding rock of the underground chamber, and a reliable channel for calculating the ultimate failure load of the surrounding rock of the chamber is provided by the limit analysis method [5–9]. The subsidence range of the overlying coal seam in the roadway under the influence of mining based on the key layer theory was predicted by Sun et al. [10], and the movement and failure laws of the coal seam were revealed. The upper bound

theorem and H-B strength criterion were combined by Wang et al. [11], whose influence was studied on different parameters of the roof collapse range of rectangular chambers and circular chambers. The high-order element adaptive upper bound finite element method was constructed by Sun et al. [12], whose failure mode and upper bound solution of the tunnel were studied. Aimed at the deep chamber in unsaturated soil, the upper bound method and the nonlinear M-C failure criterion were combined by Zhao et al. [13], and the safety factor of a deep chamber was obtained. An improved failure mechanism of surrounding rock in underground chambers was constructed by Zhang et al. [14] under the kinematic theory of the upper bound theorem. Liu et al. [15] proposed the Baker failure criterion in the constructed underground chamber failure model, and the potential collapse range of the underground chamber was predicted. The two-dimensional finite multi-block translational failure model of loess tunnels was constructed for the pore water effect by Yu et al. [16], and the overall safety factor of tunnels and the corresponding slip surface were solved. Huang et al. [17] considered the influence of the hidden karst cave formed by groundwater erosion on the chamber, the two-dimensional collapse failure mechanism of underground chambers with the karst cave was established, and the roof failure shape and scope of underground chambers were studied to be induced by the hidden karst cave via the upper bound method.

None of the above research has considered the parameter randomness effect on the underground chamber stability, but the rock and soil parameter is often very random in practical engineering. Therefore, some scholars have merged the limit analysis method and reliability theory for the stability evaluation of underground chambers [18,19]. The random response surface method was applied to these velocity fields by Mollon et al. [20], and the failure probability was computed when the shield tunnel face was unstable. The randomness of rock and soil parameters was considered by Zhang et al. [21–23], and the optimal support force range of shield tunnel faces was obtained by the response surface method. The tunnel face failure mechanisms were constructed by Pan and Dias [24] via the upper bound method, and the failure probability variation of tunnel faces was studied under the influence of randomness and spatial variability. A stochastic limit method was proposed by Cheng et al. [25], and its influence on reliability and failure probability under different soil conditions was discussed through parameter analysis. The critical safety distance of double shallow buried tunnels was explored by Zhang et al. [26], and the safety factors of different safety distances for double shallow buried tunnels were analyzed by the reliability theory. The supporting effect and parameter uncertainty of the rock roadway support system were considered by Lü et al. [27], the rock roadway support system reliability with various failure modes through the response surface method. Luo and Li [28] combined with the upper bound method of nonlinear failure criteria, the effect of the different parameter variability on the failure probability of underground chambers by the response surface method.

The above studies rarely consider the nonlinear characteristics of geotechnical materials, pore water effects and parameter randomness at the same time, and it is difficult to accurately and comprehensively analyze the stability of underground chambers under natural geological conditions. In this paper, comprehensively considering the nonlinear failure characteristics of geotechnical materials and pore water effect, the surrounding rock pressure of underground chambers is calculated by the upper bound method of limit analysis, and the influence of various random parameters on the reliability of underground chambers is studied according to the narrow boundary method of the correlation of multiple failure modes. It is expected to give a new method for accurately analyzing the safety of surrounding rock in underground chambers.

2. Upper Bound Method under the Pore Water Pressure

To investigate the influence of pore water pressure on geotechnical engineering stability, Viratjandr and Michalowski [29] regarded pore water pressure as an external force load and introduced it into the upper bound calculation of limit analysis. Because of the

simple calculation process and clear physical meaning of this method, this method has been widely used in the study of the pore water effect on the stability of geotechnical engineering. The work done by the pore water pressure mainly occurs on the soil mass skeleton and on the discontinuity of the failure body in the motion permitting velocity field. Since the failure mechanism is treated as a rigid body in the calculation, the pore water power P_u is as follows:

$$P_u = - \int_S u_i n_i v_i dS \quad (1)$$

In the above formula, u_i is the pore water pressure, v_i is the velocity field at any point in the failure body, n_i is the normal vector on the velocity discontinuity of the failure body and S is the boundaries of the failure body.

The upper bound theorem under the pore water pressure is as follows [30]:

$$\int_V \sigma_{ij} \dot{\epsilon}_{ij} dV \geq \int_S T_i v_i dS + \int_V F_i v_i dV - \int_S u_i n_i v_i dS \quad (2)$$

In the preceding formula, σ_{ij} is the stress tensor, T_i is the surface force on the boundary, F_i is the volume force, $\dot{\epsilon}_{ij}$ is the volumetric strain rate of the failure body and V is the failure body volume.

3. Hoek-Brown Failure Criterion

Hoek and Brown [31,32] obtained the final expression of the Hoek-Brown failure criterion through numerous rock mechanics experiments and field tests of rock mass, and after constant correction and improvement:

$$\sigma_1 = \sigma_3 + \sigma_{ci} \left(m_b \frac{\sigma_3}{\sigma_1} + S \right)^a \quad (3)$$

In the formula: σ_1 and σ_3 represent the maximum principal stress and the minimum principal stress when the rock mass is damaged, respectively, and σ_{ci} represents the uniaxial compressive strength. m_b , S and a are all dimensionless parameters. The three expressions are as follows:

$$m_b = m_i \exp \left(\frac{GSI - 100}{28 - 14D} \right) \quad (4)$$

$$S = \exp \left(\frac{GSI - 100}{9 - 3D} \right) \quad (5)$$

$$\alpha = \frac{1}{2} + \frac{1}{6} \left(e^{-GSI/15} - e^{-20/3} \right) \quad (6)$$

In the above formula, m_i is the rock mass constant, GSI is the geological strength index to characterize the structural integrity of rock mass and D is the disturbance factor. For the upper bound solution of underground chambers under the Hoek-Brown failure criterion, the “tangent method” should be used to obtain its supporting force, in which the relationship between c_t and φ_t can be written as [33,34]:

$$\frac{c_t}{\sigma_{ci}} = \frac{\cos \varphi_t}{2} \left[\frac{m_b a (1 - \sin \varphi_t)}{2 \sin \varphi_t} \right]^{\frac{a}{1-a}} - \frac{\tan \varphi_t}{m_b} \left(1 + \frac{\sin \varphi_t}{a} \right) \left[\frac{m_b a (1 - \sin \varphi_t)}{2 \sin \varphi_t} \right]^{\frac{1}{1-a}} + \frac{s}{m_b} \tan \varphi_t \quad (7)$$

In the preceding formula, the internal friction angle φ_t is optimized by the principle of minimum energy consumption when calculating the upper limit, and c_t is obtained by Equation (7) after φ_t is determined.

4. Calculation of the Upper Bound Solution of Surrounding Rock Pressure

4.1. Failure Mode and Velocity Field

The failure mode of underground chambers proposed in reference [14] did not consider the comprehensive influence of pore water and nonlinear characteristics of geotechnical materials, and the results often had a certain deviation from the actual engineering. In order to overcome this shortcoming, the basic requirements of the upper bound theorem are combined in the paper. When considering the pore water effect and the nonlinearity of geotechnical materials, the failure mechanism consisting of “Downward sliding wedge-shaped collapse body + Rotating circular arc body with the vertex angle as the center of a circle + Three translational triangles” is established. As seen in Figure 1 below.

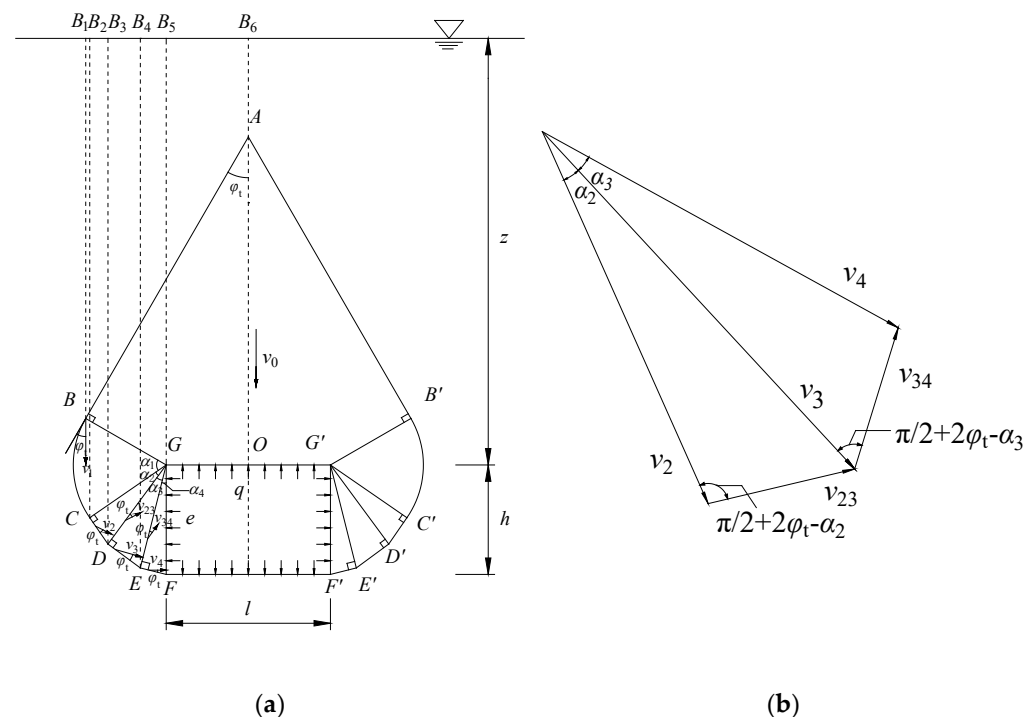


Figure 1. Failure mode and velocity vector of underground chambers under pore water effect: (a) Failure mode; (b) Velocity vector.

As in Figure 1a, since the failure mechanism is symmetrical about the center line, half of the destruction mechanism can be used for derivation and calculation. In all the calculation formulas below, γ represents the rock mass gravity, c_t represents the rock mass cohesion, φ_t is the internal friction angle, l is the chamber width, h is the chamber height, z is the water level line height, q is the roof supporting force (the surrounding rock pressure), e is the two gangs supporting force and K represents the lateral pressure coefficient. α_1 , α_2 , α_3 and α_4 are angles.

4.2. Calculation Process

4.2.1. Calculation of Velocity Field in Underground Chamber Failure Mode

By analyzing the rotating circular arc body and the velocity vector connection between each failure block in Figure 1, it can be seen that:

$$v_2 = v_1 \cdot e^{\alpha_1 \tan 2\varphi_t} = v_0 \cdot e^{\alpha_1 \tan 2\varphi_t} \quad (8)$$

$$v_{23} = \frac{\sin \alpha_2}{\cos 2\varphi_t} v_2 \quad (9)$$

$$W_4 = \gamma \cdot S_{GDE} \cdot v_3 \cdot \cos\left(\frac{\pi}{2} + \varphi_t - \alpha_1 - \alpha_2\right) = \gamma \cdot \frac{1}{2} GD \cdot DE \cdot v_3 \cdot \sin(\alpha_3 + \alpha_4 - \varphi_t) = \gamma h^2 v_0 f_4 \quad (19)$$

$$f_4 = \frac{1}{2} \sin \alpha_3 \cdot \cos \alpha_3 \cdot \cos^2 \alpha_4 \cdot \frac{\cos(2\varphi_t - \alpha_2)}{\cos 2\varphi_t} \cdot e^{\alpha_1 \tan 2\varphi_t} \cdot \sin(\alpha_3 + \alpha_4 - \varphi_t) \quad (20)$$

The triangular rigid block GEF :

$$W_5 = \gamma \cdot S_{GEF} \cdot v_4 \cdot \cos\left(\frac{\pi}{2} + \varphi_t - \alpha_4\right) = \gamma \cdot \frac{1}{2} GE \cdot EF \cdot v_4 \cdot \sin(\alpha_4 - \varphi_t) = \gamma h^2 v_0 f_5 \quad (21)$$

$$f_5 = \frac{1}{2} \sin \alpha_4 \cdot \cos \alpha_4 \cdot \frac{\cos(2\varphi_t - \alpha_3) \cdot \cos(2\varphi_t - \alpha_2)}{\cos^2 2\varphi_t} e^{\alpha_1 \tan 2\varphi_t} \cdot \sin(\alpha_4 - \varphi_t) \quad (22)$$

2. Pore water power

According to Equation (1), all the work done by the pore water pressure occurs on the velocity discontinuity line. The total power of pore water pressure can be obtained by accumulating the pore water power on all velocity discontinuity lines.

(1) The length of each auxiliary line is calculated as follows:

$$B_1 B_6 = AB \cdot \sin \varphi_t \quad (23)$$

$$AB_6 = OB_6 - AO \quad (24)$$

$$B_1 B = AB \cdot \cos \varphi_t + AB_6 \quad (25)$$

$$B_1 B_5 = BG \cdot \sin(\alpha_1 + \alpha_2 + \alpha_3 + \alpha_4) \quad (26)$$

$$B_2 C = z + CG \cdot \cos(\alpha_2 + \alpha_3 + \alpha_4) \quad (27)$$

$$B_2 B_5 = CG \cdot \sin(\alpha_2 + \alpha_3 + \alpha_4) \quad (28)$$

$$B_3 D = z + DG \cdot \cos(\alpha_3 + \alpha_4) \quad (29)$$

$$B_1 B_3 = CD \cdot \sin\left(\frac{\pi}{2} - \alpha_2 - \alpha_3 - \alpha_4\right) \quad (30)$$

$$B_3 B_5 = DG \cdot \sin(\alpha_3 + \alpha_4) \quad (31)$$

$$B_4 E = z + EG \cdot \cos(\alpha_4) \quad (32)$$

$$B_3 B_4 = DE \cdot \sin\left(\frac{\pi}{2} - \alpha_3 - \alpha_4\right) \quad (33)$$

$$B_4 B_5 = EG \cdot \sin(\alpha_4) \quad (34)$$

(2) The power of pore water pressure on each velocity discontinuity line is as follows:
The power of pore water pressure in the discontinuity line AB as:

$$P_{u1} = \frac{1}{2} \gamma \cdot r_u \cdot v_0 \cdot \sin \varphi_t \cdot (AB_6 + BB_1) \cdot B_1 B_6 = \gamma \cdot r_u \cdot v_0 \cdot f_{u1} \quad (35)$$

$$f_{u1} = \frac{\sin \varphi_t}{2} \cdot [2z - 2h \cdot \cos \alpha_2 \cdot \cos \alpha_3 \cdot \cos \alpha_4 \cdot \sin \varphi_t - \left(\frac{h \cdot \cos \alpha_2 \cdot \cos \alpha_3 \cdot \cos \alpha_4}{\tan \varphi_t} + \frac{l}{2 \sin \varphi_t} \right) \cdot \left(\frac{h \cdot \cos \alpha_2 \cdot \cos \alpha_3 \cdot \cos \alpha_4}{\tan \varphi_t} + \frac{l}{2 \sin \varphi_t} \right) \cdot \sin \varphi_t] \quad (36)$$

The power of pore water pressure in the discontinuity line BG as:

$$P_{u2} = \frac{1}{2} \gamma \cdot r_u \cdot v_1 \cdot \sin \varphi_t \cdot (B_5G + BB_1) \cdot B_1B_5 = \gamma \cdot r_u \cdot v_0 \cdot f_{u2} \quad (37)$$

$$f_{u2} = \frac{h \cdot \sin \varphi_t}{2} \cdot (2z - h \cdot \cos \alpha_2 \cdot \cos \alpha_3 \cdot \cos \alpha_4 \cdot \sin \varphi_t) \cdot \cos \alpha_2 \cdot \cos \alpha_3 \cdot \cos \alpha_4 \cdot \sin(\alpha_1 + \alpha_2 + \alpha_3 + \alpha_4) \quad (38)$$

The power of pore water pressure in the discontinuity line CG as:

$$P_{u3} = \frac{1}{2} \gamma \cdot r_u \cdot v_2 \cdot \sin \varphi_t \cdot (B_5G + B_2C) \cdot B_2B_5 = \gamma \cdot r_u \cdot v_0 \cdot f_{u3} \quad (39)$$

$$f_{u3} = \frac{1}{2} e^{\alpha_1 \cdot \tan 2\varphi_t} \cdot \sin \varphi_t \cdot [2z + h \cdot \cos \alpha_2 \cdot \cos \alpha_3 \cdot \cos \alpha_4 \cdot \cos(\alpha_2 + \alpha_3 + \alpha_4)] \cdot [h \cdot \cos \alpha_2 \cdot \cos \alpha_3 \cdot \cos \alpha_4 \cdot \sin(\alpha_2 + \alpha_3 + \alpha_4)] \quad (40)$$

The power of pore water pressure in the discontinuity line BC as:

$$P_{u4} = \gamma \cdot r_u \cdot v_0 \cdot \sin \varphi \cdot f_{u4} \quad (41)$$

$$f_{u4} = h \cdot \cos \alpha_2 \cdot \cos \alpha_3 \cdot \cos \alpha_4 \cdot \sin \varphi_t \cdot \left\{ \frac{z}{\tan 2\varphi_t} (e^{\alpha_1 \cdot \tan 2\varphi_t}) + \frac{h \cdot \cos \alpha_2 \cdot \cos \alpha_3 \cdot \cos \alpha_4}{1 + \tan^2(2\varphi_t)} \cdot [-e^{\alpha_1 \cdot \tan 2\varphi_t} \cdot \cos(\alpha_1 - \varphi_t) + \cos \varphi_t + \tan 2\varphi_t \cdot e^{\alpha_1 \cdot \tan 2\varphi_t} \cdot \sin(\alpha_1 - \varphi_t) + \tan 2\varphi_t \cdot \sin \varphi_t] \right\} \quad (42)$$

The power of pore water pressure in the discontinuity line CD as:

$$P_{u5} = \frac{1}{2} \gamma \cdot r_u \cdot v_2 \cdot \sin \varphi \cdot (B_2C + B_3D) \cdot B_2B_3 = \gamma \cdot r_u \cdot v_0 \cdot f_{u5} \quad (43)$$

$$f_{u5} = \frac{1}{2} e^{\alpha_1 \cdot \tan 2\varphi_t} \cdot \sin \varphi_t \cdot [2z + h \cdot \cos \alpha_2 \cdot \cos \alpha_3 \cdot \cos \alpha_4 \cdot \cos(\alpha_2 + \alpha_3 + \alpha_4) + h \cdot \cos \alpha_3 \cdot \cos \alpha_4 \cdot \cos(\alpha_3 + \alpha_4)] \cdot [h \cdot \cos \alpha_3 \cdot \cos \alpha_4 \cdot \sin \alpha_2 \cdot \sin(\frac{\pi}{2} - \alpha_2 - \alpha_3 - \alpha_4)] \quad (44)$$

The power of pore water pressure in the discontinuity line DG as:

$$P_{u6} = \frac{1}{2} \gamma \cdot r_u \cdot v_{23} \cdot \sin \varphi_t \cdot (B_3D + B_5G) \cdot B_3B_5 = \gamma \cdot r_u \cdot v_0 \cdot f_{u6} \quad (45)$$

$$f_{u6} = \frac{1}{2} e^{\alpha_1 \cdot \tan 2\varphi_t} \cdot \sin \varphi_t \cdot \frac{\sin \alpha_2}{\cos 2\varphi_t} [2z + h \cdot \cos \alpha_3 \cdot \cos \alpha_4 \cdot \cos(\alpha_3 + \alpha_4)] \cdot [h \cdot \cos \alpha_3 \cdot \cos \alpha_4 \cdot \sin(\alpha_3 + \alpha_4)] \quad (46)$$

The power of pore water pressure in the discontinuity line DE as:

$$P_{u7} = \frac{1}{2} \gamma \cdot r_u \cdot v_3 \cdot \sin \varphi_t \cdot (B_3D + B_4E) \cdot B_3B_4 = \gamma \cdot r_u \cdot v_0 \cdot f_{u7} \quad (47)$$

$$f_{u7} = \frac{1}{2} e^{\alpha_1 \cdot \tan 2\varphi_t} \cdot \sin \varphi_t \cdot \frac{\cos(2\varphi_t - \alpha_2)}{\cos 2\varphi_t} \cdot [2z + h \cdot \cos \alpha_3 \cdot \cos \alpha_4 \cdot \cos(\alpha_3 + \alpha_4) + h \cdot \cos^2(\alpha_4)] \cdot [h \cdot \cos \alpha_4 \cdot \sin \alpha_3 \cdot \sin(\frac{\pi}{2} - \alpha_3 - \alpha_4)] \quad (48)$$

The power of pore water pressure in the discontinuity line GE as:

$$P_{u8} = \frac{1}{2} \gamma \cdot r_u \cdot v_{34} \cdot \sin \varphi_t \cdot (B_4E + B_5G) \cdot B_4B_5 = \gamma \cdot r_u \cdot v_0 \cdot f_{u8} \quad (49)$$

$$f_{u8} = \frac{1}{2} e^{\alpha_1 \cdot \tan 2\varphi_t} \cdot \sin \varphi_t \cdot \frac{\sin \alpha_3}{\cos 2\varphi_t} \cdot \frac{\cos(2\varphi_t - \alpha_2)}{\cos 2\varphi_t} [2z + h \cdot \cos^2(\alpha_4)] \cdot h \cdot \cos \alpha_4 \cdot \sin \alpha_4 \quad (50)$$

The power of pore water pressure in the discontinuity line EF as:

$$P_{u9} = \frac{1}{2} \gamma \cdot r_u \cdot v_4 \cdot \sin \varphi_t \cdot (B_4E + B_5F) \cdot B_4B_5 = \gamma \cdot r_u \cdot v_0 \cdot f_{u9} \quad (51)$$

$$f_{u9} = \frac{1}{2} e^{\alpha_1 \cdot \tan \varphi_t} \sin \varphi_t \cdot \frac{\cos(2\varphi_t - \alpha_3)}{\cos 2\varphi_t} \cdot \frac{\cos(2\varphi_t - \alpha_2)}{\cos 2\varphi_t} \left[2z + h \cdot \cos^2(\alpha_4) + h \right] \cdot h \cdot \cos \alpha_4 \cdot \sin \alpha_4 \quad (52)$$

3. Support pressure power

$$\begin{aligned} W_T &= -q \cdot \frac{l}{2} \cdot v_0 - e \cdot h \cdot v_4 \cdot \sin(\alpha_4 - \varphi_t) \\ &= -q \cdot \frac{l}{2} \cdot v_0 - Kq \cdot h \cdot \frac{\cos(2\varphi_t - \alpha_3) \cdot \cos(2\varphi_t - \alpha_2)}{\cos^2 2\varphi_t} e^{\alpha_1 \tan 2\varphi_t} \cdot v_0 \cdot \cos(\alpha_4 - \varphi_t) \\ &= -qv_0 h f_6 \end{aligned} \quad (53)$$

In the above formula:

$$e = Kq \quad (54)$$

$$f_6 = \frac{l}{2h} + K \cdot \frac{\cos(2\varphi_t - \alpha_3) \cdot \cos(2\varphi_t - \alpha_2)}{\cos^2 2\varphi_t} e^{\alpha_1 \tan 2\varphi_t} \cdot \cos(\alpha_4 - \varphi_t) \quad (55)$$

4. External total power

To sum up, the external total power W_{ext} can be expressed as:

$$W_{\text{ext}} = \gamma h^2 v_0 (f_1 + f_2 + f_3 + f_4 + f_5) + \gamma \cdot r_u \cdot v_0 \cdot (f_{u1} + f_{u2} + f_{u3} + f_{u4} + f_{u5} + f_{u6} + f_{u7} + f_{u8} + f_{u9}) - qh v_0 f_6 \quad (56)$$

4.2.3. Internal Energy Dissipation Power

The energy dissipation power along the discontinuity line AB as:

$$D_{AB} = c_t \cdot AB \cdot v_0 \cdot \cos \varphi_t = \left(\frac{h \cdot \cos \alpha_2 \cdot \cos \alpha_3 \cdot \cos \alpha_4}{\tan \varphi_t} + \frac{l}{2 \sin \varphi_t} \right) \cdot c_t \cdot v_0 \cdot \cos \varphi_t = c_t \cdot v_0 \cdot h \cdot f_7 \quad (57)$$

$$f_7 = \left(\frac{\cos \alpha_2 \cdot \cos \alpha_3 \cdot \cos \alpha_4}{\tan \varphi_t} + \frac{l}{2h \sin \varphi_t} \right) \cdot \cos \varphi_t \quad (58)$$

The internal energy dissipation power in the discontinuity surface BC of the rotating circular arc body and the failure region as:

$$D_{BC} = \frac{c_t \cdot BG \cdot v_1 \cdot \cos \varphi_t}{\tan 2\varphi_t} (e^{\alpha_1 \cdot \tan 2\varphi_t} - 1) = c_t h v_0 f_8 \quad (59)$$

$$f_8 = \frac{\cos \alpha_4 \cos \alpha_3 \cos \alpha_2 \cdot \cos \varphi_t}{\tan 2\varphi_t} (e^{\alpha_1 \cdot \tan 2\varphi_t} - 1) \quad (60)$$

$$D_{GBC} = \frac{c_t \cdot BG \cdot v_1 \cdot \cos \varphi_t}{\sin 2\varphi_t} (e^{\alpha_1 \cdot \tan 2\varphi_t} - 1) = c_t h v_0 f_9 \quad (61)$$

$$f_9 = \frac{\cos \alpha_4 \cos \alpha_3 \cos \alpha_2 \cdot \cos \varphi_t}{\sin 2\varphi_t} (e^{\alpha_1 \cdot \tan 2\varphi_t} - 1) \quad (62)$$

The energy dissipation power along the discontinuity line CD as:

$$D_{CD} = c_t \cdot CD \cdot v_2 \cdot \cos \varphi_t = c_t h v_0 f_{10} \quad (63)$$

$$f_{10} = \sin \alpha_2 \cos \alpha_3 \cos \alpha_4 \cdot e^{\alpha_1 \tan 2\varphi_t} \cdot \cos \varphi_t \quad (64)$$

The energy dissipation power along the discontinuity line GD as:

$$D_{GD} = c_t \cdot GD \cdot v_{23} \cdot \cos \varphi_t = c_t h v_0 f_{11} \quad (65)$$

$$f_{11} = \frac{\sin \alpha_2 \cos \alpha_3 \cos \alpha_4 \cos \varphi_t}{\cos 2\varphi_t} e^{\alpha_1 \tan 2\varphi_t} \quad (66)$$

The energy dissipation power along the discontinuity line DE as:

$$D_{DE} = c_t \cdot DE \cdot v_3 \cdot \cos \varphi_t = c_t h v_0 f_{12} \quad (67)$$

$$f_{12} = \frac{\cos(2\varphi_t - \alpha_2) \sin \alpha_3 \cos \alpha_4 \cos \varphi_t}{\cos 2\varphi_t} e^{\alpha_1 \tan 2\varphi_t} \quad (68)$$

The energy dissipation power along the discontinuity line GE as:

$$D_{GE} = c_t \cdot GE \cdot v_{34} \cdot \cos \varphi_t = c_t h v_0 f_{13} \quad (69)$$

$$f_{13} = \frac{\cos \varphi \cos \alpha_4 \sin \alpha_3 \cos(2\varphi_t - \alpha_2)}{\cos^2 2\varphi_t} e^{\alpha_1 \tan 2\varphi_t} \quad (70)$$

The energy dissipation power along the discontinuity line EF as:

$$D_{EF} = c_t \cdot EF \cdot v_4 \cdot \cos \varphi_t = c_t h v_0 f_{14} \quad (71)$$

$$f_{14} = \frac{\sin \alpha_4 \cos \varphi_t \cos(2\varphi_t - \alpha_3) \cos(2\varphi_t - \alpha_2)}{\cos^2 2\varphi_t} e^{\alpha_1 \tan 2\varphi_t} \quad (72)$$

To sum up, the internal energy dissipation total power D_{int} can be expressed as:

$$D_{\text{int}} = c_t h v_0 \cdot (f_7 + f_8 + f_9 + f_{10} + f_{11} + f_{12} + f_{13} + f_{14}) \quad (73)$$

4.2.4. Calculation of Support Force

According to the virtual work principle, the analytical formula of the roof supporting force q (the surrounding rock pressure) can be expressed as:

$$q = \frac{\gamma \cdot h \cdot (f_1 + f_2 + f_3 + f_4 + f_5) + \gamma \cdot r_u / h \cdot (f_{u1} + f_{u2} + f_{u3} + f_{u4} + f_{u5} + f_{u6})}{f_6} + \frac{\gamma \cdot r_u / h \cdot (f_{u7} + f_{u8} + f_{u9}) - c_t \cdot (f_7 + f_8 + f_9 + f_{10} + f_{11} + f_{12} + f_{13} + f_{14})}{f_6} \quad (74)$$

4.3. Reliability Model

The failure of the roof or sidewall of the underground chamber is seen as the failure of the structural system of the underground chamber. A situation in which only one failure occurs between the roof or sidewall of the underground chamber is called a single failure mode. The situation in which the roof and sidewall failures of the underground chamber are considered at the same time is called multiple failure modes. When analyzing the structural system reliability of underground chambers, it is vital to clarify the limit states of different failure modes and the correlation between them. Hence, it is more scientific and logical to investigate the stability of the underground chambers by using the wide boundary method and narrow boundary method with multiple failure modes [35]. Meanwhile, compared with the wide boundary method and the narrow boundary method, because the correlation between failure modes was considered while considering the different failure modes of the chamber by the narrow boundary method, the results obtained are better than the wide boundary method [36]. Therefore, the reliability of the underground chamber was mainly studied based on the narrow boundary method of the correlation of multiple failure modes in the paper.

4.3.1. Limit State Equation

According to Equation (74) and $e = Kq$, the expressions of e is:

$$e = Kq = K \frac{\gamma \cdot h \cdot (f_1 + f_2 + f_3 + f_4 + f_5) + \gamma \cdot r_u / h \cdot (f_{u1} + f_{u2} + f_{u3} + f_{u4} + f_{u5} + f_{u6})}{f_6} + K \frac{\gamma \cdot r_u / h \cdot (f_{u7} + f_{u8} + f_{u9}) - c_t \cdot (f_7 + f_8 + f_9 + f_{10} + f_{11} + f_{12} + f_{13} + f_{14})}{f_6} \quad (75)$$

Now it is assumed that the support pressure of the roof and sidewall of the underground chamber is σ_T , the functional functions of the roof and sidewall of the underground chamber are respectively:

$$\begin{aligned} g_1(X) &= \sigma_T - q \\ &= \sigma_T - \frac{\gamma \cdot h \cdot (f_1 + f_2 + f_3 + f_4 + f_5) + \gamma \cdot r_u / h \cdot (f_{u1} + f_{u2} + f_{u3} + f_{u4} + f_{u5} + f_{u6})}{f_6} \\ &\quad - \frac{\gamma \cdot r_u / h \cdot (f_{u7} + f_{u8} + f_{u9}) - c_t \cdot (f_7 + f_8 + f_9 + f_{10} + f_{11} + f_{12} + f_{13} + f_{14})}{f_6} \end{aligned} \quad (76)$$

$$\begin{aligned} g_2(X) &= \sigma_T - e \\ &= \sigma_T - K \frac{\gamma \cdot h \cdot (f_1 + f_2 + f_3 + f_4 + f_5) + \gamma \cdot r_u / h \cdot (f_{u1} + f_{u2} + f_{u3} + f_{u4} + f_{u5} + f_{u6})}{f_6} \\ &\quad - K \frac{\gamma \cdot r_u / h \cdot (f_{u7} + f_{u8} + f_{u9}) - c_t \cdot (f_7 + f_8 + f_9 + f_{10} + f_{11} + f_{12} + f_{13} + f_{14})}{f_6} \end{aligned} \quad (77)$$

In the above formula, $g_1(X)$ and $g_2(X)$ represent the functional functions, and X represents a random variable, namely $X = [\gamma, r_u, GSI, m_i, \sigma_{ci}, D, \sigma_T]$

4.3.2. Reliability Model under Multiple Failure Modes

The reliability model of the underground chamber under multiple failure modes is:

$$R_s = P\{g_1(X) = \sigma_T - q \cap g_2(X) = \sigma_T - e\} \quad (78)$$

The failure probability P_f of the underground chamber under multiple failure modes is:

$$P_f = 1 - R_s = 1 - P\{g_1(X) = \sigma_T - q \cap g_2(X) = \sigma_T - e\} \quad (79)$$

The reliability index β of the underground chamber under multiple failure modes is:

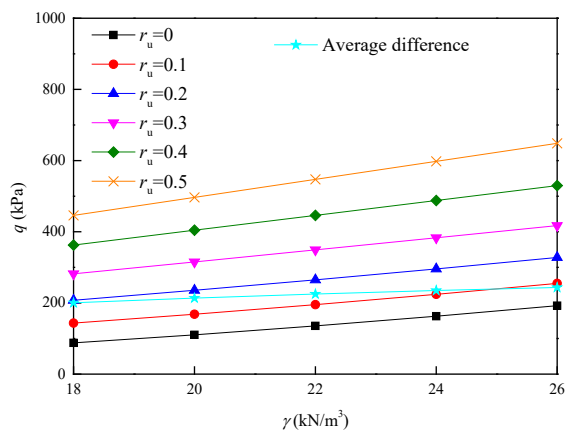
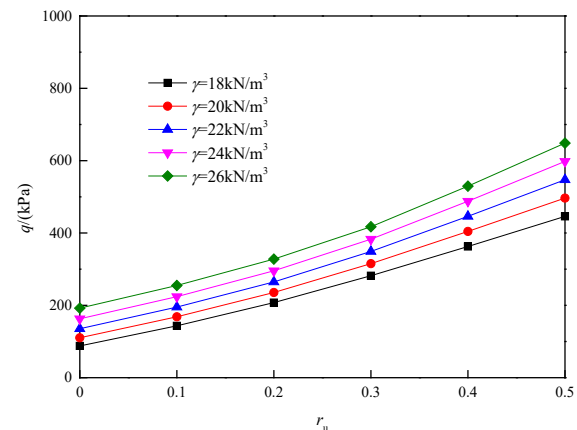
$$\beta = -\phi(P_f) = -\phi(1 - P\{g_1(X) = \sigma_T - q \cap g_2(X) = \sigma_T - e\}) \quad (80)$$

5. Comparison with or without Pore Water

In order to study the influence of the pore water effect on surrounding rock pressure q in the failure mode of underground chambers constructed in this paper, the situations without pore water ($r_u = 0$) and the situations with pore water ($r_u = 0.1$ – 0.5) are compared and analyzed. Other parameters are: $\gamma = 18$ – 26 kN/m³, $K = 1$, $l = 6$ m, $h = 5$ m, $GSI = 15$, $m_i = 10$, $\sigma_{ci} = 400$ kPa, $D = 0$ and $z = 60$ m. The calculation results of surrounding rock pressure of underground chamber under different rock mass gravity and pore water effect are shown in Table 1, and the relevant data in Table 1 are drawn in Figure 3. As shown in Figure 3, the surrounding rock pressure q of the chamber increases nonlinearly with the increase in the pore water pressure coefficient r_u . Based on the rock mass gravity $\gamma = 24$ kN/m³ as an example, the average difference between the surrounding rock pressure of the underground chamber calculated by considering pore water and the calculation result without pore water is 234.91 kPa, the average difference of surrounding rock pressure under different pore water pressure coefficients of other groups is both more than 200 kPa. The analysis shows that the existence of pore water will have a considerable impact on the surrounding rock pressure of the underground chamber.

Table 1. Surrounding rock pressure under different pore water effects/kPa.

γ (kN/m ³)	q (kPa)						Average Difference (kPa)
	$r_u = 0$	$r_u = 0.1$	$r_u = 0.2$	$r_u = 0.3$	$r_u = 0.4$	$r_u = 0.5$	
18	87.79	143.48	207.61	281.86	362.71	445.98	200.54
20	110.47	168.39	235.60	315.31	404.36	496.60	213.58
22	135.48	195.24	264.85	349.01	446.06	547.24	225.00
24	162.76	224.10	295.55	382.99	487.82	597.91	234.91
26	192.28	254.96	327.85	417.31	529.62	648.60	243.39

(a) q - γ - r_u (b) q - r_u - γ **Figure 3.** Chart of surrounding rock pressure under different pore water effects.

6. Result Analysis

6.1. Underground Chamber Surrounding Rock Pressure without Considering Parameter Randomness

The surrounding rock pressure of underground chambers under the Hoek-Brown failure criterion and pore water was investigated without considering the randomness of parameters. Among them: $\gamma = 18 \text{ kN/m}^3$ – 26 kN/m^3 , $K = 0.6$ – 1.4 , $GSI = 10$ – 35 , $m_i = 5$ – 30 , $\sigma_{ci} = 200 \text{ kPa}$ – 1200 kPa , $D = 0$ – 0.5 , $r_u = 0$ – 0.5 , $z = 40 \text{ m}$ – 90 m and $l \times h = 6 \text{ m} \times 5 \text{ m}$. The calculation result of the surrounding rock pressure q of the underground chamber is shown in Figure 4 under various effect parameters.

When K is constant, the surrounding rock pressure q of the underground chamber increases with the increase in the rock mass gravity γ , as illustrated in Figure 4a. This indicates that we need to reinforce the support when excavating the chamber in the surrounding rock with a large weight to avoid the chamber collapsing. When the rock mass gravity γ is constant, as shown in Figure 4b, the roof pressure of the underground chamber nonlinearly decreases from steep to slow as the lateral pressure coefficient K increases. As shown in Figure 4c,d, as the geological strength index GSI and the rock mass constant m_i increase, the surrounding rock pressure q of the underground chamber decreases in a nonlinear manner. Figure 4c shows that when the geological strength index GSI increases under a certain m_i , the surrounding rock pressure of the chamber decreases significantly at first, then gradually. This is because when the GSI increases, the integrity of the rock mass improves, thereby reducing the support force necessary to maintain the stability of the chamber. Figure 4d analysis reveals that the overall changing trend is comparable to Figure 4c; when GSI is constant, as the rock mass constant m_i increases, the surrounding rock pressure in the underground chamber decreases, so does its variation rate. This reflects that the rock mass constant m_i represents the quality of the surrounding rock. When m_i is small, the surrounding rock condition is poor but, as m_i increases, the surrounding rock condition improves, the surrounding rock self-stability is enhanced, and the chamber surrounding rock pressure decreases significantly. When the disturbance factor D is

constant, the surrounding rock pressure q decreases from sharp to sluggish as the uniaxial compressive strength σ_{ci} increases, as shown in Figure 4e, and this tendency is more visible when the disturbance factor D is large. This shows that the surrounding rock with good compressive capacity has good bearing capacity and strong self-stability, and that the support force to maintain the chamber stability is more minimal. As shown in Figure 4f, when the uniaxial compressive strength σ_{ci} remains unchanged, the surrounding rock pressure q of the chamber increases nonlinearly with the growth of the disturbance factor D . The negative impacts of blasting and other vibration loads on the underground chamber should be considered throughout the excavation and design of the chamber, and the supporting measures of the chamber should be improved. When $r_u \neq 0$, that is, when the pore water effect occurs, the surrounding rock pressure q increases with the uplift of water-level line height z , as shown in Figure 4g. When the water level line height z is constant, as shown in Figure 4h, the surrounding rock pressure q of the chamber increases nonlinearly with the increase in the r_u . This suggests that the negative impact of pore water effect on the stability of surrounding rock should be considered emphatically for underground chambers excavated in water-rich layers.

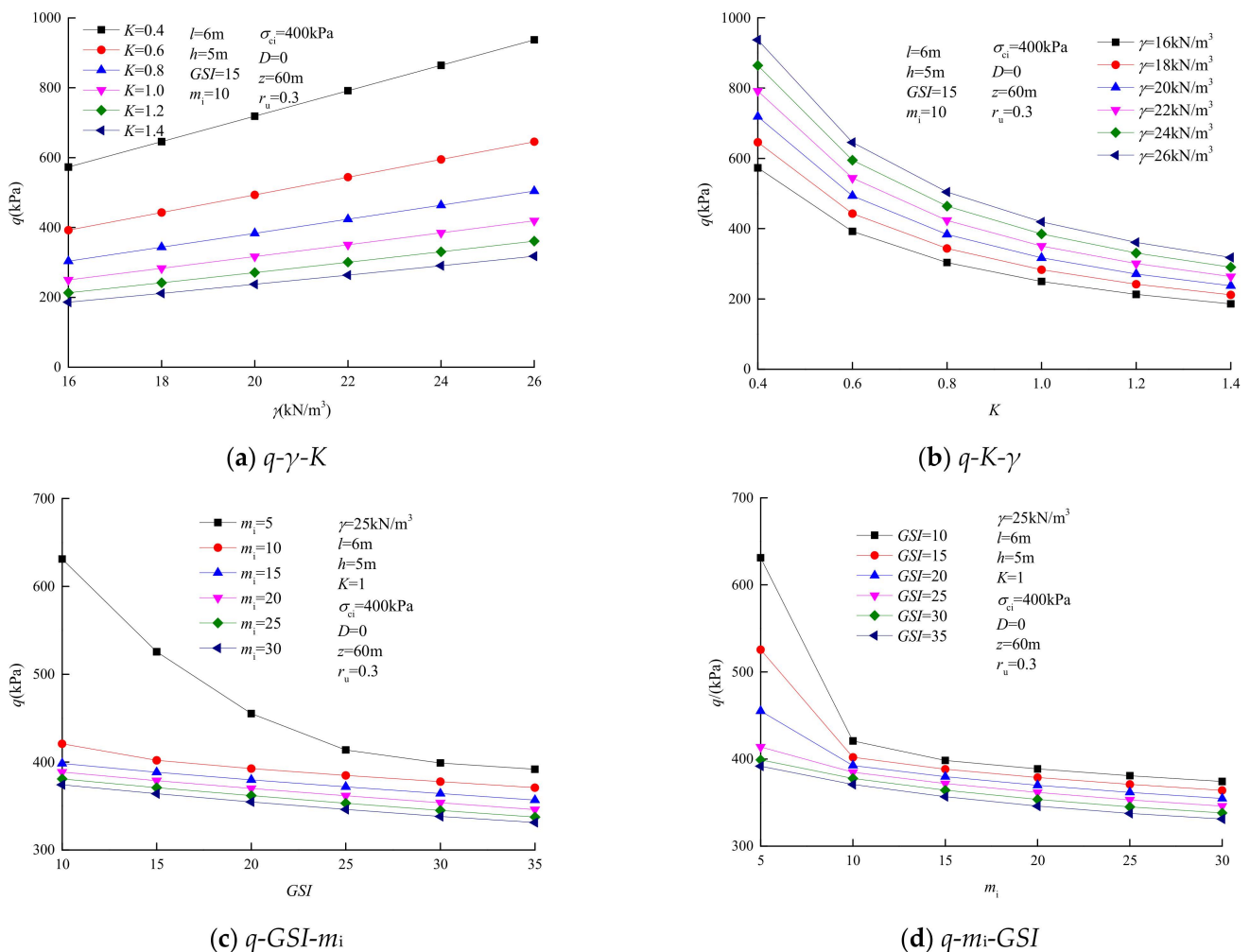


Figure 4. Cont.

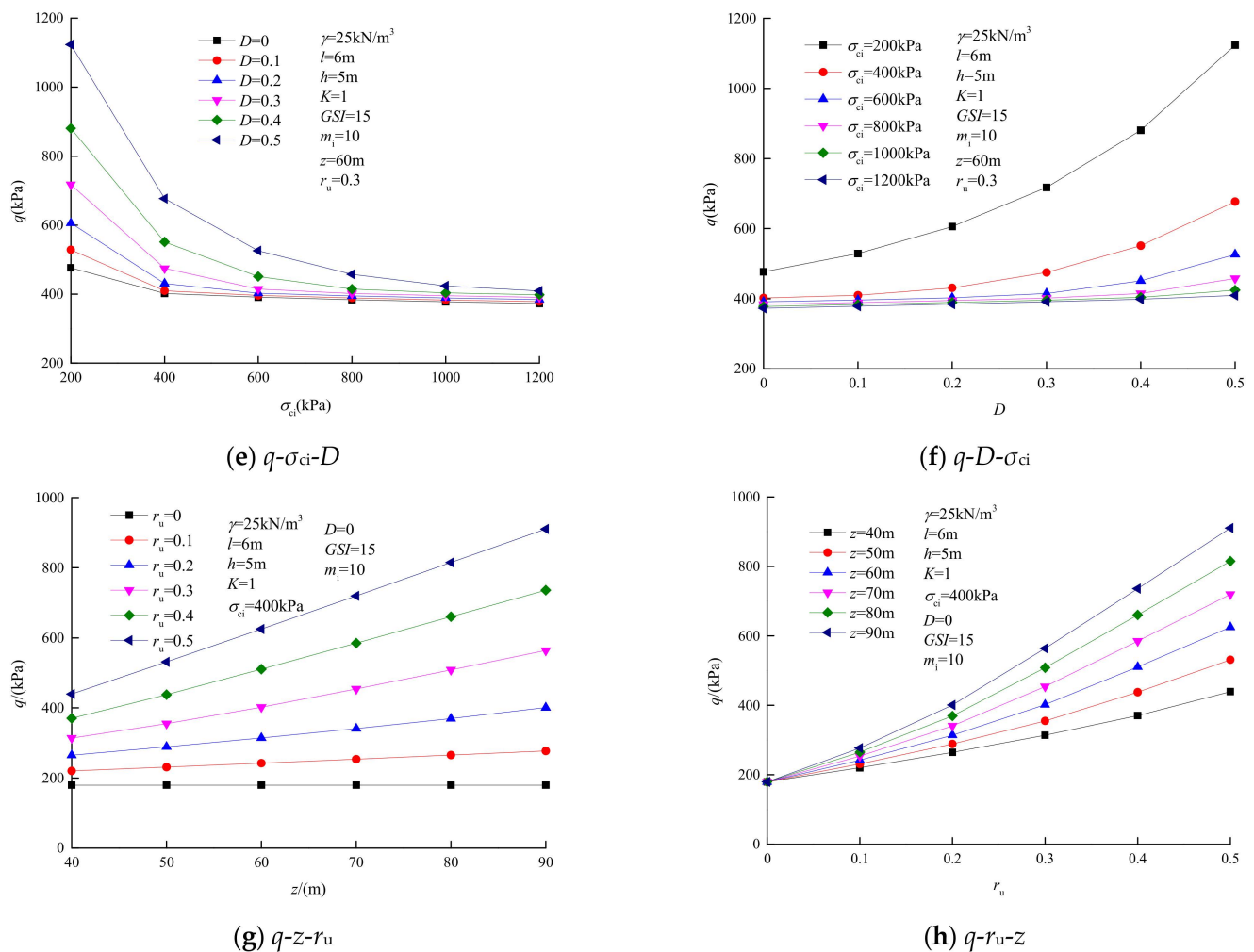


Figure 4. Influence rule of key parameters on underground chamber rock pressure.

6.2. Influence of Different Random Parameters on Underground Chamber Reliability

6.2.1. Random Variable Statistical Features

For further analysis, the reliability of underground chambers under the pore water effect on the basis of the surrounding rock pressure of underground chambers. The influence of parameter randomness is considered on the stability of underground chambers in this paper, and the failure probability P_f and reliability index β of underground chambers are analyzed based on the reliability theory by using the narrow boundary method with the correlation of multiple failure modes. When the randomness of rock parameters and supporting force have been studied, relevant scholars have determined the value range of the parameters and determined that their distribution pattern was the normal distribution [18,19,32]. Therefore, according to the existing results, it is assumed that the statistical features of the main parameters and support forces are shown in Table 2. The values of other relevant parameters are as follows: $l = 6\text{ m}$, $h = 5\text{ m}$ and $K = 1$.

Table 2. Statistical features of random variable parameters.

Random Variable Parameter	Mean Value	Standard Deviation	Coefficient of Variation	Distribution Pattern
γ (kN/m ³)	25	1.25	0.05	Normal distribution
r_u	0.3	0.06	0.20	Normal distribution
GSI	15	2.25	0.15	Normal distribution
m_i	10	1.5	0.15	Normal distribution
σ_{ci} (kPa)	400	60	0.15	Normal distribution
D	-	-	0.15	Normal distribution
σ_T (kPa)	-	-	0.15	Normal distribution

6.2.2. The Influence of Rock Mass Gravity

In order to examine the influence of rock mass gravity γ on the reliability of underground chambers, the failure probability P_f and reliability index β of underground chambers are calculated by using the narrow boundary method under different rock mass weights γ . Other relevant parameters are as follows: $l = 6$ m, $h = 5$ m, $K = 1$, $GSI = 15$, $m_i = 10$, $\sigma_{ci} = 400$ kPa, $D = 0$, $z = 60$ m and $r_u = 0.3$. Figure 5 depicts the effect of varied rock mass gravity γ on the dependability of underground chambers. According to Figure 5, the failure probability P_f of underground chambers decreases nonlinearly from steep to slow as the mean value of support force σ_T increases, and the reliability index β increases nonlinearly. The failure probability P_f of underground chambers increases as the rock mass gravity γ increases for a certain mean value of support force, but the reliable index β decreases. Therefore, it is necessary to increase the support force to maintain the stability of the chamber for the underground chamber with heavy rock mass gravity. Meanwhile, the concept of the safety level of underground chambers is introduced in Figure 5. The failure probability $P_f = 1.3 \times 10^{-5}$ or the dependability index $\beta = 4.2$ when the safety level is 1. Since the results obtained by the narrow boundary method have upper and lower boundaries, the minimum support force range required to maintain the stability of underground chambers under the influence of different rock mass gravity γ when the safety level is 1 can be obtained, as shown in Table 3. This range of support forces can serve as a theoretical basis and reference for underground chamber design. Furthermore, when analyzing whether the case of parameter randomness is considered, taking the rock mass weight $\gamma = 22$ kN/m³ as an example, when the parameters randomness is not considered, the upper bound solution of the support force of underground chambers is 349 kPa. When the parameter randomness is considered, it can be seen from Figure 5 that the corresponding support force ranges are 460–466 kPa, 586–593 kPa, 718–728 kPa and 874–887 kPa when the failure probability $P_f = 0.1$, 0.01, 0.001 and 0.0001, respectively. And the failure probability $P_f = 1.3 \times 10^{-5}$, that is, when the safety level is 1, the support force range required to maintain the stability of underground chambers is 1043–1063 kPa. To sum up, the support force range obtained when the parameter randomness is considered, is significantly larger than the support force 349 kPa obtained by the fixed value method. This shows that even with a sufficient support force, the underground chamber engineering still has a high probability of instability. On the contrary, the underground chamber engineering with an insufficient supporting force may also be in a stable state. Therefore, considering the randomness of rock parameters and external loads, the reliability theory is used for analysis, in which the actual working state of underground chamber engineering could be more accurately reflected, thereby the instability risk of underground chamber engineering was effectively reduced by increasing the size of the supporting force.

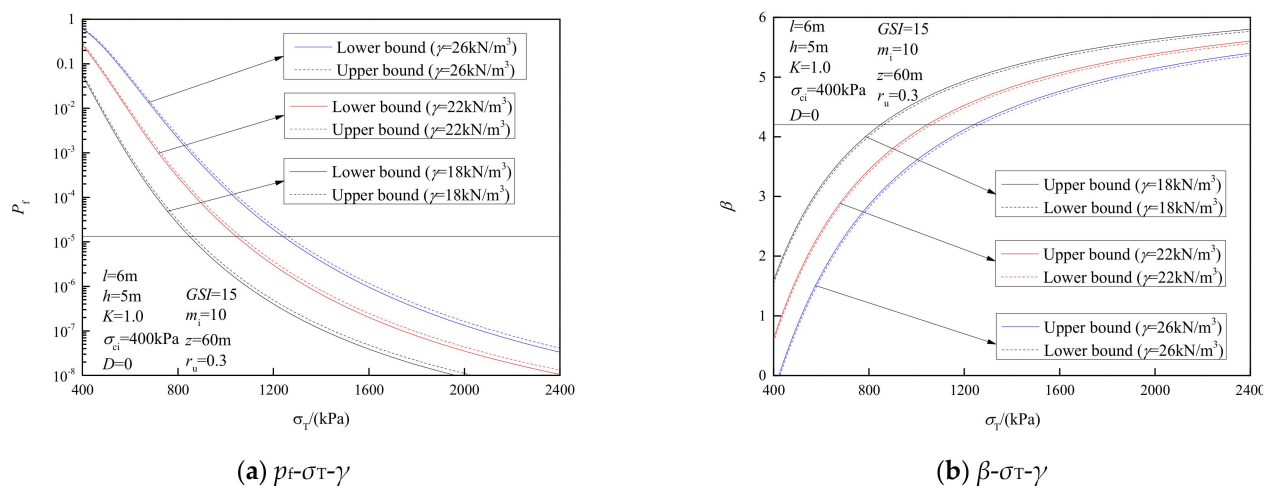


Figure 5. Influence of various rock mass gravity on the reliability of underground chambers.

Table 3. Support force range of underground chamber safety design level 1 under different rock mass gravity.

γ (kN/m ³)	Lower Bound of Narrow Boundary Method (kPa)	Upper Bound of Narrow Boundary Method (kPa)	Support Force Range (kPa)
18	848	862	[848, 862]
22	1043	1061	[1043, 1063]
26	1239	1260	[1039, 1260]

6.2.3. The Influence of Hoek-Brown Criteria Parameters

To investigate the influence of Hoek-Brown criterion parameters on the reliability of underground chambers, the failure probability P_f and reliability index β of underground chambers are calculated by using the narrow boundary method under different Hoek-Brown criterion parameters. Parameters such as GSI , m_i , σ_{ci} and D are assumed as random variables respectively. Other relevant parameters are: $\gamma = 25 \text{ kN/m}^3$, $l = 6 \text{ m}$, $h = 5 \text{ m}$, $K = 1$, $z = 60 \text{ m}$ and $r_u = 0.3$. The effect of different Hoek-Brown criteria parameters on the underground chamber reliability is depicted in Figure 6. In Figure 6, the failure probability P_f of underground chambers decreases nonlinearly as the mean value of support force σ_T increases, and the reliability index β increases rapidly at first and subsequently slowly. From Figure 6a–f, it can be observed that for a certain mean value of support force, with the increase in GSI , m_i and σ_{ci} , the failure probability P_f of underground chambers decreases and the reliability index β increases. This is due to GSI , m_i and σ_{ci} increasing, which means that the surrounding rock of the underground chamber becomes better and the self-stability of the chamber is improved. From Figure 6g–h, when the mean value of support force remains unchanged, as the disturbance factor D increases, the failure probability P_f of underground chambers increases, and the reliability index β decreases. It implies that the excavation of underground chambers is more likely to be prone to instability failure under the environment with strong disturbance factors, thus should be avoided during the excavation of underground chambers big disturbance. Meanwhile, the concept of the safety level of underground chambers is introduced in Figure 6. The minimum support force range required to maintain the stability of underground chambers under different Hoek-Brown criterion parameters can be obtained when the safety level is 1 ($P_f = 1.3 \times 10^{-5}$ or $\beta = 4.2$), and the statistics are shown in Table 4.

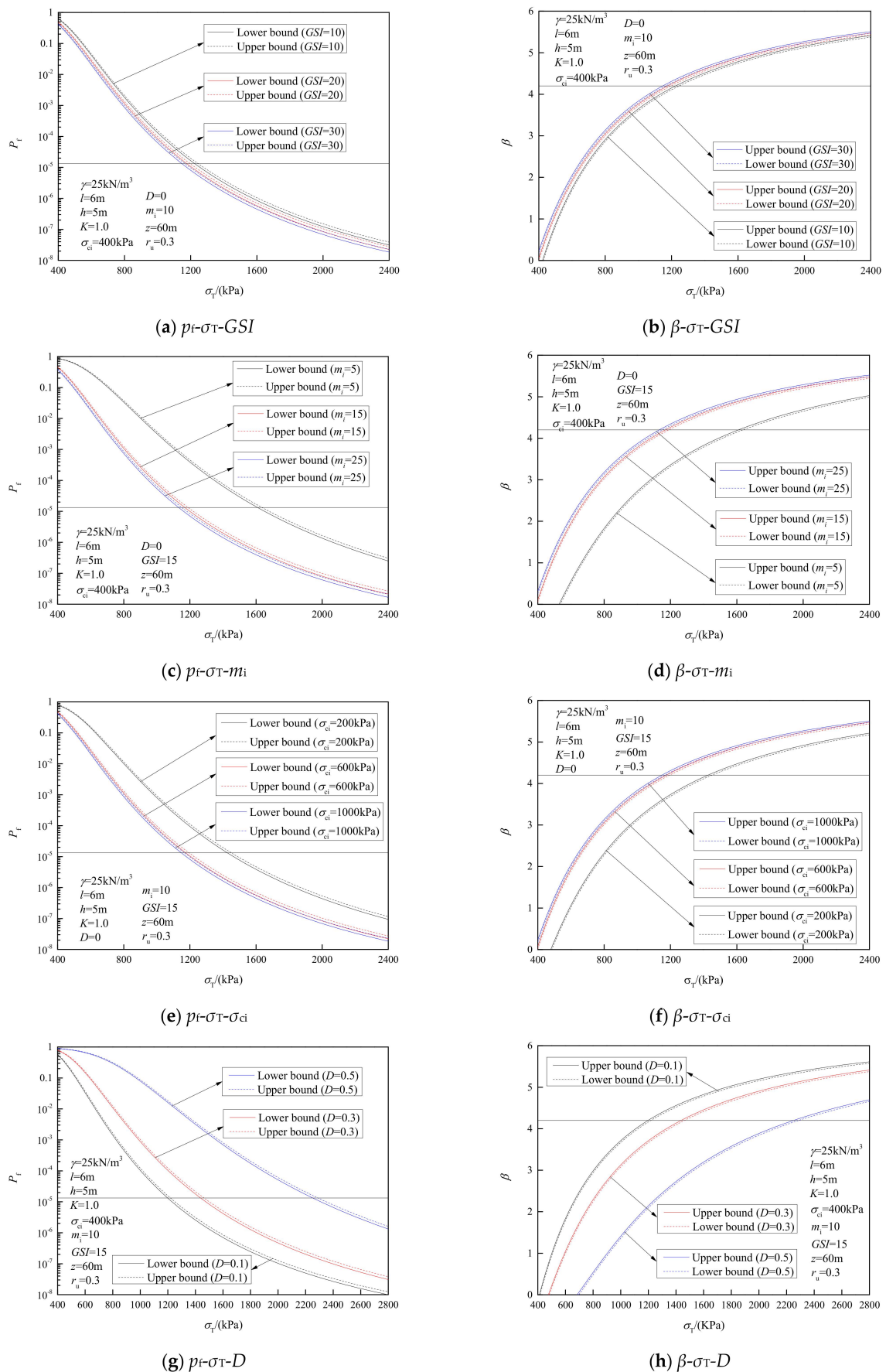


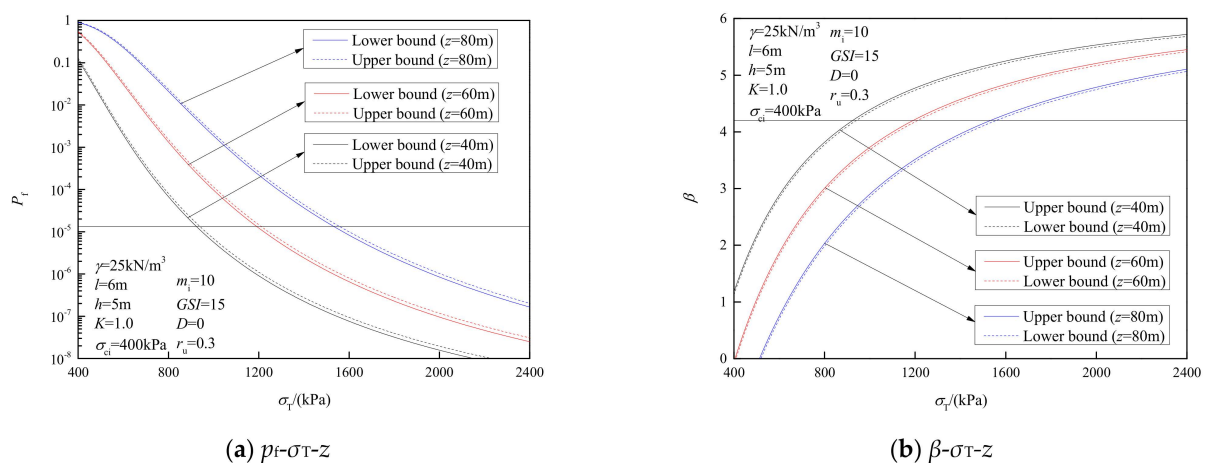
Figure 6. Influence of different Hoek-Brown criterion parameters on underground chamber reliability.

Table 4. Support force range of underground chamber safety design level 1 under different Hoek-Brown criterion parameters.

Random Variable Parameter		Lower Bound of Narrow Boundary Method (kPa)	Upper Bound of Narrow Boundary Method (kPa)	Support Force Range (kPa)
GSI	10	1224	1244	[1224, 1244]
	20	1176	1196	[1176, 1196]
	30	1146	1165	[1146, 1165]
	5	1609	1636	[1609, 1636]
m_i	15	1167	1187	[1167, 1187]
	25	1132	1149	[1132, 1149]
	200	1425	1449	[1425, 1449]
σ_{ci}/kPa	600	1174	1195	[1174, 1195]
	1000	1147	1167	[1147, 1167]
	0.1	1197	1218	[1197, 1218]
D	0.3	1437	1461	[1437, 1461]
	0.5	2251	2287	[2251, 2287]

6.2.4. The Influence of Pore Water

In order to examine the influence of pore water on the reliability of underground chambers, the failure probability P_f and reliability index β of underground chambers are calculated by using the narrow boundary method under different water level line heights z and pore water pressure coefficient r_u respectively. Other parameters are as follows: $\gamma = 25 \text{ kN/m}^3$, $l = 6 \text{ m}$, $h = 5 \text{ m}$, $K = 1$, $GSI = 15$, $m_i = 10$, $\sigma_{ci} = 400 \text{ kPa}$ and $D = 0$. The effect of various water level line heights z and pore water pressure coefficient r_u on the reliability of underground chambers is depicted in Figure 7. As Figure 7, the failure probability P_f of underground chambers decreases nonlinearly as the mean value of support force σ_T increases, whereas the reliability index β increases nonlinearly. Figure 7a–d show that the failure probability P_f of underground chambers increases as the increase in z and r_u , but the dependable index β decreases. Therefore, the influence of pore water should be properly considered in the design of the underground chamber rich in groundwater, and an effective scheme of precipitation and drainage should be formulated. During construction, real-time monitoring of pore water should be strengthened to avoid the destruction of underground chambers due to excessive pore water pressure. Moreover, the concept of the safety level of underground chambers is introduced in Figure 7. The minimum support force range required to maintain the stability of underground chambers under different water level line heights z and pore water pressure coefficient r_u can be obtained when the safety level is 1 ($P_f = 1.3 \times 10^{-5}$ or $\beta = 4.2$), and the statistics are shown in Table 5.

**Figure 7.** Cont.

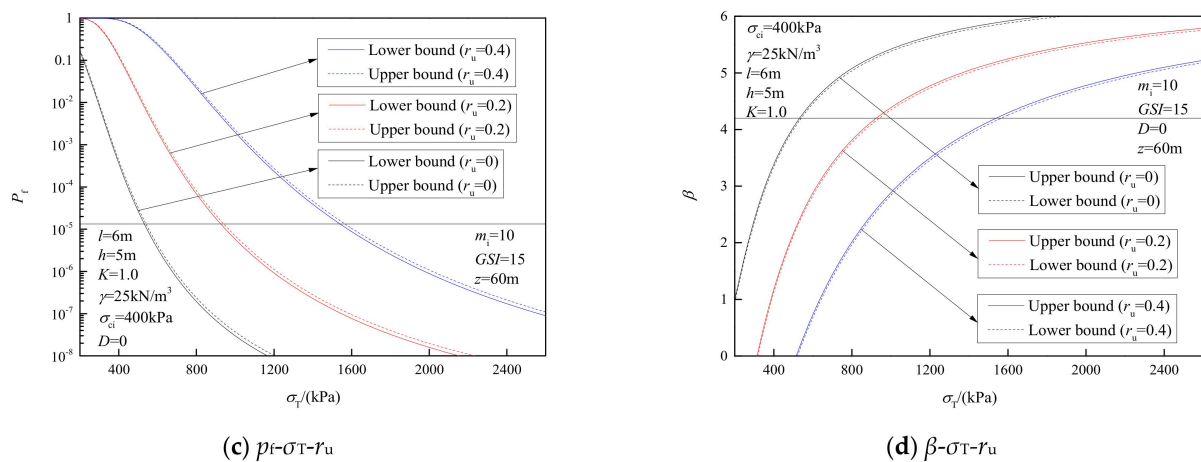


Figure 7. Influence of various water level line heights and pore water pressure coefficients on underground chamber reliability.

Table 5. Support force range of underground chamber safety design level 1 under various water level line heights and pore water pressure coefficients.

Random Variable Parameter		Lower Bound of Narrow Boundary Method (kPa)	Upper Bound of Narrow Boundary Method (kPa)	Support Force Range (kPa)
z/m	40	923	939	[923, 939]
	60	1191	1211	[1191, 1211]
	80	1533	1557	[1533, 1557]
r_u	0	532	540	[532, 540]
	0.2	925	941	[925, 941]
	0.4	1539	1565	[1539, 1565]

7. Conclusions

- By comparing the situation with and without pore water, it is concluded that the existence of pore water will have a considerable impact on the surrounding rock pressure, and the average difference of the surrounding rock pressure of the underground chamber under different pore water pressure coefficients is more than 200 KPa.
- When parameter randomness is not considered, the surrounding rock pressure q of underground chambers increases with the increase in the rock mass gravity γ , while the roof pressure of underground chambers decreases with the increase in the lateral pressure coefficient K . For the Hoek-Brown failure criterion parameters, the surrounding rock pressure q of underground chambers decreases nonlinearly with the increase in the GSI , m_i and σ_{ci} , and shows a nonlinear increasing trend with the increase in D . For pore water, the rise of z and the increase in r_u will lead to an increase in the surrounding rock pressure q of the chamber. Therefore, the influence of pore water should be fully considered in the design of the underground chamber rich in groundwater, and an effective scheme of precipitation and drainage should be formulated.
- Based on the narrow boundary method of the correlation of multiple failure modes, the reliability of underground chambers is analyzed under the influence of different random parameters. With the increase in σ_T , the failure probability P_f of underground chambers decreases nonlinearly from steep to slow, and the reliability index β increases nonlinearly. With the increase in the γ , z and r_u , the failure probability P_f of underground chambers increases, and the reliability index β decreases. With the increase in the GSI , m_i , σ_{ci} or the decrease in D , the failure probability P_f of underground chambers decreases, and the reliability index β increases.

Author Contributions: Conceptualization, D.Z. and J.Z.; data curation, B.Y.; software, X.Y.; project administration, J.Z.; supervision, D.Z.; writing—original draft preparation, H.Y.; writing—review and editing, H.Y. All authors have read and agreed to the published version of the manuscript.

Funding: The work was funded by the National Natural Science Foundation of China, grant number 52074116 and 51804113.

Institutional Review Board Statement: Not applicable.

Informed Consent Statement: Not applicable.

Data Availability Statement: Not applicable.

Conflicts of Interest: All authors declare that they have no conflict of interest or financial conflict to disclose.

References

1. Xie, C.; Nguyen, H.; Bui, X.-N.; Nguyen, V.-T.; Zhou, J. Predicting roof displacement of roadways in underground coal mines using adaptive neuro-fuzzy inference system optimized by various physics-based optimization algorithms. *J. Rock Mech. Geotech. Eng.* **2021**, *13*, 1452–1465. [\[CrossRef\]](#)
2. Xie, C.; Nguyen, H.; Choi, Y.; Armaghani, D.J. Optimized functional linked neural network for predicting diaphragm wall deflection induced by braced excavations in clays. *Geosci. Front.* **2022**, *13*, 101313. [\[CrossRef\]](#)
3. Weng, L.; Wu, Q.-H.; Zhao, Y.-L.; Wang, S.-M. Dynamic response and failure of rock in initial gradient stress field under stress wave loading. *J. Cent. South Univ.* **2020**, *27*, 963–972. [\[CrossRef\]](#)
4. Wu, Q.-H.; Weng, L.; Zhao, Y.-L.; Feng, F. Influence of infilling stiffness on mechanical and fracturing responses of hollow cylindrical sandstone under uniaxial compression tests. *J. Central South Univ.* **2021**, *28*, 2485–2498. [\[CrossRef\]](#)
5. Fraldi, M.; Guarracino, F. Limit analysis of collapse mechanisms in cavities and tunnels according to the Hoek–Brown failure criterion. *Int. J. Rock Mech. Min. Sci.* **2009**, *46*, 665–673. [\[CrossRef\]](#)
6. Yang, X.-L.; Li, Z.-W.; Liu, Z.-A.; Xiao, H.-B. Collapse analysis of tunnel floor in karst area based on Hoek–Brown rock media. *J. Central South Univ.* **2017**, *24*, 957–966. [\[CrossRef\]](#)
7. Zhang, J.-H.; Zhang, B. Reliability analysis for seismic stability of tunnel faces in soft rock masses based on a 3D stochastic collapse model. *J. Central South Univ.* **2019**, *26*, 1706–1718. [\[CrossRef\]](#)
8. Zhang, D.; Zhang, B. Stability Analysis of the Pressurized 3D Tunnel Face in Anisotropic and Nonhomogeneous Soils. *Int. J. Géoméch.* **2020**, *20*, 1–18. [\[CrossRef\]](#)
9. Zhang, D.-B.; Ma, Z.-Y.; Yu, B.; Yin, H.-D. Upper bound solution of surrounding rock pressure of shallow tunnel under nonlinear failure criterion. *J. Central South Univ.* **2019**, *26*, 1696–1705. [\[CrossRef\]](#)
10. Sun, Y.; Zuo, J.; Karakus, M.; Liu, L.; Zhou, H.; Yu, M. A New Theoretical Method to Predict Strata Movement and Surface Subsidence due to Inclined Coal Seam Mining. *Rock Mech. Rock Eng.* **2021**, *54*, 2723–2740. [\[CrossRef\]](#)
11. Wang, H.; Liu, P.; Wang, L.G.; Liu, C.; Zhang, X.; Liu, L. Three-Dimensional Collapse Analysis for a Shallow Cavity in Layered Strata Based on Upper Bound Theorem. *Comput. Model. Eng. Sci.* **2020**, *124*, 375–391. [\[CrossRef\]](#)
12. Sun, R.; Yang, J.-S.; Zhao, Y.-D.; Yang, F. Upper bound adaptive finite element method with higher-order element based on Drucker–Prager yield criterion. *Chin. J. Geotech. Eng.* **2020**, *42*, 398–404. [\[CrossRef\]](#)
13. Zhao, Y.; Li, X.; Tai, P.; Huang, L.; Pu, B.; Chen, R. Upper bound limit analysis of roof collapse of deep cavities in unsaturated soils. *Int. J. Numer. Anal. Methods Géoméch.* **2022**, *46*, 1224–1240. [\[CrossRef\]](#)
14. Zhang, D.-B.; Liu, Z.-Z.; Zhang, J.-H. A new failure mechanism for deep cavity and upper bound solution of supporting pressure. *J. Central South Univ.* **2017**, *24*, 2082–2091. [\[CrossRef\]](#)
15. Liu, Z.-Z.; Cao, P.; Lin, H.; Meng, J.-J.; Wang, Y.-X. Three-dimensional upper bound limit analysis of underground cavities using nonlinear Baker failure criterion. *Trans. Nonferrous Met. Soc. China* **2020**, *30*, 1916–1927. [\[CrossRef\]](#)
16. Yu, L.; Lv, C.; Wang, Z.-H.; Sun, Y.; Yang, N.; Wang, Z.-L.; Wang, M.-N. Upper Bound Analysis of Collapse Failure in Deep Buried Tunnel under upper Cave. *China J. Highw. Transp.* **2021**, *34*, 209–219. [\[CrossRef\]](#)
17. Huang, F.; Zhang, M.; Jiang, Z. Collapse mode of rock mass induced by a concealed karst cave above a deep cavity. *J. Central South Univ.* **2019**, *26*, 1747–1754. [\[CrossRef\]](#)
18. Zhang, B.; Ma, Z.-Y.; Wang, X.; Zhang, J.-S.; Peng, W.-Q. Reliability analysis of anti-seismic stability of 3D pressurized tunnel faces by response surfaces method. *Geomech. Eng.* **2020**, *20*, 43–54. [\[CrossRef\]](#)
19. Zhang, D.; Sun, W.; Wang, C.; Yu, B. Reliability Analysis of Seismic Stability of Shield Tunnel Face under Multiple Correlated Failure Modes. *KSCE J. Civ. Eng.* **2021**, *25*, 3172–3185. [\[CrossRef\]](#)
20. Mollon, G.; Dias, D.; Soubra, A.-H. Range of the Safe Retaining Pressures of a Pressurized Tunnel Face by a Probabilistic Approach. *J. Geotech. Geoenvironmental Eng.* **2013**, *139*, 1954–1967. [\[CrossRef\]](#)
21. Zhang, J.-H.; Wang, W.-J.; Zhang, D.-B.; Zhang, B.; Meng, F. Safe Range of Retaining Pressure for Three-dimensional Face of Pressurized Tunnels based on Limit Analysis and Reliability Method. *KSCE J. Civ. Eng.* **2018**, *22*, 4645–4656. [\[CrossRef\]](#)

22. Zhang, J.; Zhang, L.; Wang, W.; Zhang, D.; Zhang, B. Probabilistic analysis of three-dimensional tunnel face stability in soft rock masses using Hoek–Brown failure criterion. *Int. J. Numer. Anal. Methods Géoméch.* **2020**, *44*, 1601–1616. [[CrossRef](#)]
23. Zhang, J.-H.; Xu, P.; Sun, W.-C.; Li, B. Seismic reliability analysis of shield tunnel faces under multiple failure modes by pseudo-dynamic method and response surface method. *J. Cent. South Univ.* **2022**, *29*, 1553–1564. [[CrossRef](#)]
24. Pan, Q.; Dias, D. Probabilistic evaluation of tunnel face stability in spatially random soils using sparse polynomial chaos expansion with global sensitivity analysis. *Acta Geotech.* **2017**, *12*, 1415–1429. [[CrossRef](#)]
25. Cheng, H.-Z.; Chen, J.; Chen, R.-P.; Chen, G.-L. Reliability study on shield tunnel face using a random limit analysis method in multilayered soils. *Tunn. Undergr. Space Technol.* **2019**, *84*, 353–363. [[CrossRef](#)]
26. Zhang, B.; Wang, X.; Zhang, J.-S.; Cheng, H. Safe range analysis of clear distance of twin shallow tunnels based on limit analysis and reliability theory. *J. Central South Univ.* **2018**, *25*, 196–207. [[CrossRef](#)]
27. Lü, Q.; Xiao, Z.-P.; Ji, J.; Zheng, J. Reliability based design optimization for a rock tunnel support system with multiple failure modes using response surface method. *Tunn. Undergr. Space Technol.* **2017**, *70*, 1–10. [[CrossRef](#)]
28. Luo, W.-H.; Li, W.-T. Reliability analysis of supporting pressure in tunnels based on three-dimensional failure mechanism. *J. Central South Univ.* **2016**, *23*, 1243–1252. [[CrossRef](#)]
29. Viratjandr, C.; Michalowski, R.L. Limit analysis of submerged slopes subjected to water drawdown. *Can. Geotech. J.* **2006**, *43*, 802–814. [[CrossRef](#)]
30. Zhang, J.-H.; Wang, W.-J.; Zhang, B.; Zhang, D.-B. Upper Bound Analysis for Collapse Failure of Shield Tunnel Face Excavated in Unsaturated Soils Considering Steady Vertical Flow. *Math. Probl. Eng.* **2019**, *2019*, 1–10. [[CrossRef](#)]
31. Hoek, E.; Brown, E.T. Empirical Strength Criterion for Rock Masses. *J. Geotech. Eng. Div.* **1980**, *106*, 1013–1035. [[CrossRef](#)]
32. Hoek, E.; Brown, E. Practical estimates of rock mass strength. *Int. J. Rock Mech. Min. Sci.* **1997**, *34*, 1165–1186. [[CrossRef](#)]
33. Huang, F.; Zhang, D.-B.; Sun, Z.-B.; Wu, B. Influence of pore water pressure on upper bound analysis of collapse shape for square tunnel in Hoek–Brown media. *J. Central South Univ.* **2011**, *18*, 530–535. [[CrossRef](#)]
34. Zhang, B.; Jiang, J.; Zhang, D.-B.; Liu, Z. Upper bound solution of collapse pressure and permanent displacement of 3D tunnel faces using the pseudo-dynamic method and the kinematic approach. *Geomech. Eng.* **2021**, *25*, 521–533. [[CrossRef](#)]
35. Zhang, M. *Structural Reliability Analysis: Methods and Procedures*; Science Publishing & Media Group Ltd.: Beijing, China, 2009.
36. Zhang, B. *Three-Dimensional Stability Analysis and Reliability Study of Tunnel Faces Using upper Bound Method*; Central South University: Changsha, China, 2018.